


Research Article

A Neural Network-Based Ionospheric Electron Density Model over an African Equatorial Region Centered in Kano, Nigeria, Using COSMIC Mission Data

Sani Abubakar^{1, 2, *} , Daniel Okoh^{3, 4}, Bello Idrith Tijjani¹, Rabia Salihu Said¹, Benjamin Ayantunji Gbenro², Enoch O. Elemo²

¹Department of Physics, Bayero University, Kano, Nigeria

²Department of Physical and Life Science, National Space Research and Development Agency, Abuja, Nigeria

³Istituto Nazionale Geofisica e Vulcanologia (INGV), Roma, Italy

⁴United Nations African Regional Centre for Space Science and Technology Education in English (UN-ARCSSTE-E), Ile-Ife, NARDA, Nigeria

Abstract

This study focuses on modeling the ionospheric electron density over a 5 degree rectangular African equatorial region centered in Kano, Nigeria, using artificial neural network. The electron density measurements data used in this research were obtained from the Constellation Observing System for Meteorology Ionosphere and Climate (COSMIC) team covering the period of 16 years ranging from 2006 to 2021 through the method of radio occultation. The data is in *ionPrf* file format provided by the COSMIC team. The profiles are in *netCDF* format containing ionospheric information including electron density profiles. The data were collected from a 5-degree rectangular African equatorial region centered in Kano, Nigeria (geographic coordinates: 12.00°N, 8.59°E; geomagnetic coordinates: 0.47°N). Computer neural network was used in training the data using the Levenberg Marquardt (LM) algorithm. Results for 22 trained networks demonstrated that the network with nineteen hidden layer neurons gave the most accurate result with root-mean square error (RMSE) of 86×10^3 electrons per cubic centimeter. The criteria was that the best network is the one that gives the highest minimization of RMSE. The nineteenth network was therefore finally used as the neural network (NN) electron density model. The NN model's hourly binned electron density predictions was compared with those of the NeQuick and International Reference Ionosphere (IRI) models. The result of the comparison illustrated that out of the 423 investigated ionosonde profiles, the NN model performed best in 200 profiles (approximately 47%) followed by the IRI which performed best in 114 profiles (approximately 27%) while the NeQuick performed best in 109 profiles (approximately 26%). The developed NN model was demonstrated to be able to reproduce the different ionospheric features (diurnal variations, seasonal variations, and the long-term changes).

Keywords

COSMIC Mission, Electron Density, Ionosphere, Neural Network, Radio Occultation, Ionosonde

*Corresponding author: sani.abubakar46@yahoo.com (Sani Abubakar)

Received: 9 November 2024; **Accepted:** 17 December 2024; **Published:** 30 December 2024



Copyright: © The Author(s), 2024. Published by Science Publishing Group. This is an **Open Access** article, distributed under the terms of the Creative Commons Attribution 4.0 License (<http://creativecommons.org/licenses/by/4.0/>), which permits unrestricted use, distribution and reproduction in any medium, provided the original work is properly cited.

1. Introduction

The ionosphere (a layer with a series of regions) ranges from 50–1000 km above the surface of the earth [28] with high electron density sufficient to influence electromagnetic wave propagation due to the considerable amount of charged particles content in it [26]. Refraction and signal delays are among the major phenomena affecting the trans-ionospheric radio waves propagation such as radio waves signal in which changes in the ionosphere's density and composition can disrupt these signals. One of the most popular equipment used to study ionospheric variability has been the Global Navigation Satellite System (GNSS) ground-based receivers. This equipment is however sparsely distributed in Nigeria, and by extension, the African equatorial region [22]. The launch of the Constellation Observing System for Meteorology, Ionosphere, and Climate (COSMIC) satellites in 2006 (COSMIC 1) and in 2019 (COSMIC 2) have enabled improvement in accuracy of ionospheric investigations and modeling, especially in parts of the globe (such as equatorial Africa) where ground-based equipment are scarce [11]. The relative positioning between the COSMIC satellites and the GPS satellites also gives room for determining electron density profiles present in the ionosphere [14] by the method of radio occultation. Lots of efforts have been put into trying to understand and model the ionosphere thus leading to continuous updates of the global ionospheric models. One of the accurate methods of studying the ionosphere is the use of the ionosonde [12]. The ionospheric electron densities measured by the Ilorin ionosonde (IL008), Nigeria (geographic coordinates: 8.5 °N, 4.5 °E; geomagnetic coordinates: 1.8°S), which is entirely a different dataset, were used, in this research, for validation. However, recent studies (over Nigeria) have focused on modeling the ionospheric total electron content (TEC) like [17, 19, 20, 22, 24]. The electron density parameter offers many advantages, especially for modelling ionospheric and space weather. The electron density provides a three-dimensional view of the ionosphere (latitude, longitude, and altitude) which is important for fully understanding of the vertical structure of the ionospheric variability at different altitudes.

The disastrous positioning errors caused by the ionosphere led to continues updates of global ionospheric models. Some of the most popular and globally used ionospheric models include: the IRI [5-8] and the NeQuick [18]. However, recent studies (over Nigeria) are focused on modeling the ionospheric TEC like [17, 19, 20, 22, 24] using data from the Global Positioning System (GPS) accessed through GPS ground-based receivers which are even sparsely distributed in Nigeria.

The launch of COSMIC 1 satellites in 2006 and COSMIC 2 satellites in 2019 enables improvement in the accuracy of ionospheric modeling especially the African equatorial region where the ground-based receivers are sparsely distributed. Some of these models include, [4, 11, 13, 14, 21, 23]. Computer neural network has increasingly become a very useful

tool in modeling the ionosphere due to many of its important characteristics. Some of these characteristics include its ability to handle a very large amount of data, learn its patterns, and predict future trends in the data [22]. Some neural network-based ionospheric models include [11, 19, 22, 23]. Since training artificial neural networks has to use one of the basic learning algorithms and the best model selection depends on the best choice of algorithm in terms of accuracy and speed [3, 9]. This research employed the Levenberg Marquardt algorithm, which is the best of the algorithms in terms of combination of accuracy and speed [1, 3, 9] and is therefore the frequently used algorithm [2, 19, 22, 24].

The aim of this research is therefore to develop ionospheric electron density model using radio occultation-based electron density observations from COSMIC team, and artificial neural network. The model is able to: (i) overcome the problem of discontinuity (in time) of the COSMIC dataset over the selected region (which is one of the limitations of the COSMIC data) by deriving continuous electron density values over the region and (ii) reproduce different features of the ionosphere over the equatorial region when compared to an entirely different dataset.

2. Materials and Methods

2.1. Data

For this research, the COSMIC satellite data used for the development of these model were obtained from the University Corporation for Atmospheric Research (UCAR) in 'ionPrf' file format. These data are the netCDF format second-level profiles provided by the COSMIC group. The profiles contain electron density measurements by Radio Occultation (RO) technique during the period 2006 through 2021. Only the electron density measurements within the 5-degree rectangular region around Kano (geographic coordinates: 12.00°N, 8.59°E; geomagnetic coordinates: 0.47°N) were used. The number of data points used in the development of the model was about 2,885,337 data points collected from around the Kano region. The research also used ionosonde data from Ilorin station, IL008 (geographic: 8.5 °N, 4.5 °E; geomagnetic coordinates: 1.8 °S) for validation purposes. Before the use of the COSMIC data the following data quality control was performed [11] (a) all negative electron density values were removed; (b) all profiles containing negative electron density values at altitudes equal to or above 100 km were removed; (c) all profiles with peak electron densities (hmF2) not in the range 200-550 km were also removed. Hourly disturbed disturbance storm time (Dst) and solar activity at a wavelength of 10.7 cm (F10.7) indices used were obtained from the OMNIWeb of NASA's Goddard Space Flight Center.

This work employs employed neural network method of modeling due to its many important characteristics and having

the capacity to handle a very large amount of data, and also its ability to learn data patterns and predict future trends in the data computer neural network has recently become a very useful tool in modeling the ionosphere. The neural network is also able to overcome one of the limitations of COSMIC satellite measurements that the measurements are not continuous in time over any given Earth location but when trained using historical COSMIC satellite measurements over a given Earth location, they can learn temporal variations in the data, and can therefore be used to derive values that are continuous in time over the location. Neural network is also chosen to investigate the idea that neural networks are suitable candidates for contemporary ionospheric modeling in this era of big data.

The MATLAB function 'ncread' was used to extract the altitudinal electron density profiles from the netCDF files. The region, which lies well within the African equatorial trough region, is shown in Figure 1.

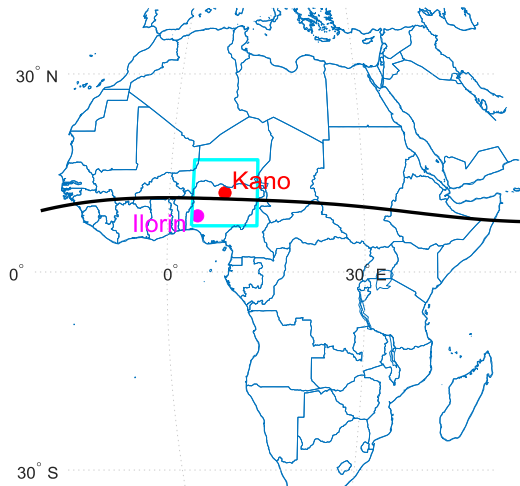


Figure 1. Map of Africa indicating the area of the research. From Figure 1, the red dot represents the location of Kano (geographic coordinates: 12.00° N, 8.59° E; geomagnetic coordinates: 0.47° N) whereas the majestic dot represents the location of Ilorin station, IL008, Nigeria (geographic coordinates: 8.5°N, 4.5°E; geomagnetic coordinates: 1.8°S). The rectangle represents the area of the 5-degree rectangular region around the location, including Ilorin, Nigeria. The black line running across the map represents the geomagnetic equator.

2.2. The Neural Network Inputs

The artificial neural network mainly has three input layer matrices: the input layer matrix (I_m), the hidden layer matrix (H_m), and the output layer matrix (O_m). The input layer matrix contains inputs fed into the network, the hidden layer matrix is the matrix in which the intermediate values are computed and the output layer matrix is the matrix that contains the desired or target outputs from the neural network. The neural network's input layer was fed with relevant inputs that enabled the network to learn the trend and pattern of the

data for prediction. The altitude for each profile of electron density was used as an input. For the network to learn diurnal and seasonal variations, the hour of the day (hr) and day of the year (doy) were considered. Since the ionosphere also changes over a relatively long time, the network was fed with flux with 10.7 cm wavelength (F10.7) to learn long-term electron density changes determined by solar activity. The disturbance storm time (Dst) index was also used as input to represent ionospheric dynamics caused by geomagnetic storm influence.

The two cyclical components of the hour of the day (hr) and day of the year (doy) i.e. the sine and cosine components as described by equations (1) and (2) for hr and equations (3) and (4) for doys was to allow for a numerically continuous trend in the data [11, 23].

$$doy_s = \sin\left(\frac{2\pi \times doy}{365.25}\right) \quad (1)$$

$$doy_c = \cos\left(\frac{2\pi \times doy}{365.25}\right) \quad (2)$$

$$hr_s = \sin\left(\frac{2\pi \times hr}{24}\right) \quad (3)$$

$$hr_c = \cos\left(\frac{2\pi \times hr}{24}\right) \quad (4)$$

From the foregoing, it summarily indicated that the final neural network training was run using the following 9 input neurons doy_s , doy_c , hr_s , hr_c , altitude, longitude, latitude, F10.7 and Dst.

Normalization of the training data was done using the mapminmax processing function, which is default for MATLAB neural network trainings [15]. The mapminmax function normalizes the training data so that inputs fall in the range [-1, 1] by mapping the minimum and the maximum values to -1 and 1, respectively [16].

2.3. Training Procedure of the Neural Networks

Artificial neural network can either be feedforward or recurrent neural network. The major difference between them is that unlike feedforward neural networks. Recurrent neural networks can have multiple feedback loops which can appear in many forms between any two layers or neurons. The network can have single or multiple hidden neurons layers. Another advantage of recurrent neural networks over feedforward neural networks for handling time-series and dynamical related problems is that recurrent neural networks consist of a large number of feedforward and feedback connections and therefore a smaller network size of recurrent neural networks can be equivalent to a complicated feedforward neural network architecture [27]. Another advantage include the convergence of the network and their efficient approximation capabilities which led to wide application of the recurrent neural networks. For this advantages this study employed a recurrent neural networks. The neural network training and

test were performed using radio occultation-based ionospheric electron density measurements. A neural network is normally trained to obtain a set of target outputs from the network from the applied set of inputs [22, 29]. The raining involves computation of error and adjustment of the weights from a set of inputs presented until convergence is obtained. The process continues until a specified training condition has been achieved. Training in neural network is categorized in to supervised, unsupervised and reinforcement training [10]. The commonly used type in neural network is the supervised training. In supervised training, a set of inputs is presented to the neural network with target output vectors (standard training set) aiming at simulating this standard by adjusting its weights within an appropriate error limit [10]. In unsupervised training, only input vectors are fed into the network. Since each input is generally assumed to belong to a particular class from the several classes, the network output is also assumed to be an identification of the class to which its input arises from. So the training should let the network discover hidden futures so that inputs should be grouped into classes that are found different [10]. Reinforcement training is not a commonly used training. It is a combination of the supervised and unsupervised training. In reinforcement training, no presentation of the desired outputs to the network but the network is allowed to examine its ability to simulate the input signal [10] so this research employed supervised training.

One of the most important technique for training neural networks is the error backpropagation algorithm. For each of the examples in training dataset, the algorithm calculates the error. This is done by using error function (the difference between original and predicted output). The inputs weights are adjusted by the error when propagated back over the hidden nodes. The error backpropagation process is completed after the minimum error solution is reached.

The randomly selected 85% of the data was used for the training while 15%, also randomly selected, was used for the independent test that represent 85% and 15% of the entire dataset.

The input layer matrix, I_m , containing 9 input neurons (as explained earlier) was connected to the hidden layer matrix, H_m (which computes the intermediary values) with a hyperbolic tangent-sigmoid transfer function. This transfer function is advantageous because it is differentiable and also allows for easy computation of gradient which is necessary for training through backpropagation and the output layer matrix, O_m , containing the target electron density as output from the neural network, was connected to the hidden layer matrix with a linear transfer function as described by equation the following equations.

$$H_m = \tanh(I_{wm} \times I_m + B_1) \quad (5)$$

$$O_m = H_{wm} \times H_m + B_2 \quad (6)$$

where I_{wm} is the input layer weight matrix, B_1 is the input

layer bias vector, H_{wm} is the hidden layer weight matrix, and B_2 is the hidden layer bias vector. These weight matrices and the bias vectors characterize the trained neural network and change only when the neural network is trained [11, 23].

2.4. Early Stopping Technique

Firstly, the early stopping technique was applied [25] in order to determine the optimal number of training epochs/iterations and this differ for each network training. This was achieved by dividing the 85% dataset in two disjoint subsets: the training set and the validation set. From this 85%, 70% was used for the learning itself while the 15% was used as validation which was to choose the number of training epochs. Learning ends when the error on the validation set begins to increase even if the error on the training set could further be reduced, to enable improvement in the ability of generalization of the network. To avoid occurrence of overtraining even on the validation set, a further test subset (the remaining 15% of the data) was used to assess the capacity of generalization of the network. This means the dataset has been respectively divided into three subsets: the training subset used for the learning itself, the validation subset and the test subset, by assigning them (randomly) the 70%, the 15% and the 15% of the whole data sets, respectively. The Levenberg-Marquardt algorithm, which is the best back-propagation algorithm for training data on neural networks in terms of speed and accuracy [1], was used in training 22 different networks (which differ in one neuron starting with one hidden layer neuron) in which the network with nineteen hidden layer neurons gave the minimum RMSE.

Ionosonde electron density measurements from the Ilorin (IL008) station was used for validation and to measure the performance of the NN, NeQuick, and IRI models in comparison. The RMSE i.e. the difference between the ionosonde electron density measurements and the corresponding NN, Nequick, and IRI predicted electron densities was used as a technique for measuring the performance of each of the models.

$$RMSE = \sqrt{\frac{\sum_{i=1}^n (e_i - e_p)^2}{n}} \quad (7)$$

where e_i are the ionosonde electron-density measurements, e_p are the corresponding electron density predictions from the three models, and n is the number of observations.

3. Results and Discussion

3.1. Different Networks Trained by the Levenberg Marquardt's Algorithm

The networks training using the Levenberg Marquardt algorithm stops at the network with twenty-two hidden layer neurons when the error in the validation set was noticed rising after the minimum RMSE (highest accuracy) has already been

reached. The network with nineteen hidden layer neurons exhibited minimum RMSE (highest accuracy as demonstrated

in Figure 2) and the root-mean square errors are recorded for each network.

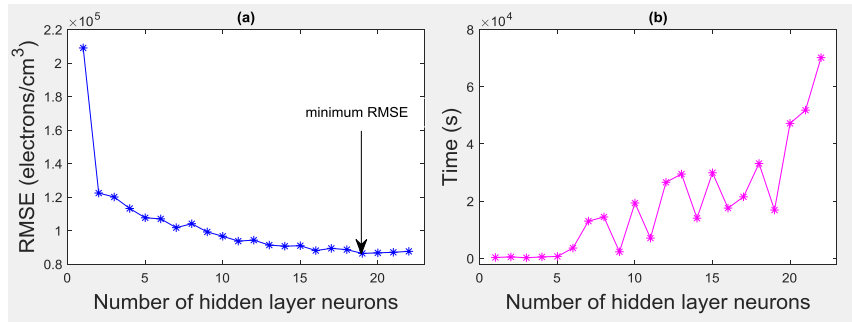


Figure 2. (a): root-mean-square errors for the twenty-two trained networks. (b): duration for each network to complete training.

3.2. Validation with Ionosonde (IL008) Measurements in Comparison to IRI and Nequick Predictions

The neural network model's performance was validated using the Ilorin-Nigeria (geographic coordinates: 8.5° N, 4.5° E; geomagnetic coordinates: 1.8° S), measurements and

compared with the IRI and NeQuick model's predictions. For comparison, the average of the electron density profiles for each month of the periods in which models' predictions coincide with periods for which ionosonde data is available for the years: 2010, 2013, 2014, and 2019 were computed see Figure 3 and Table 1.

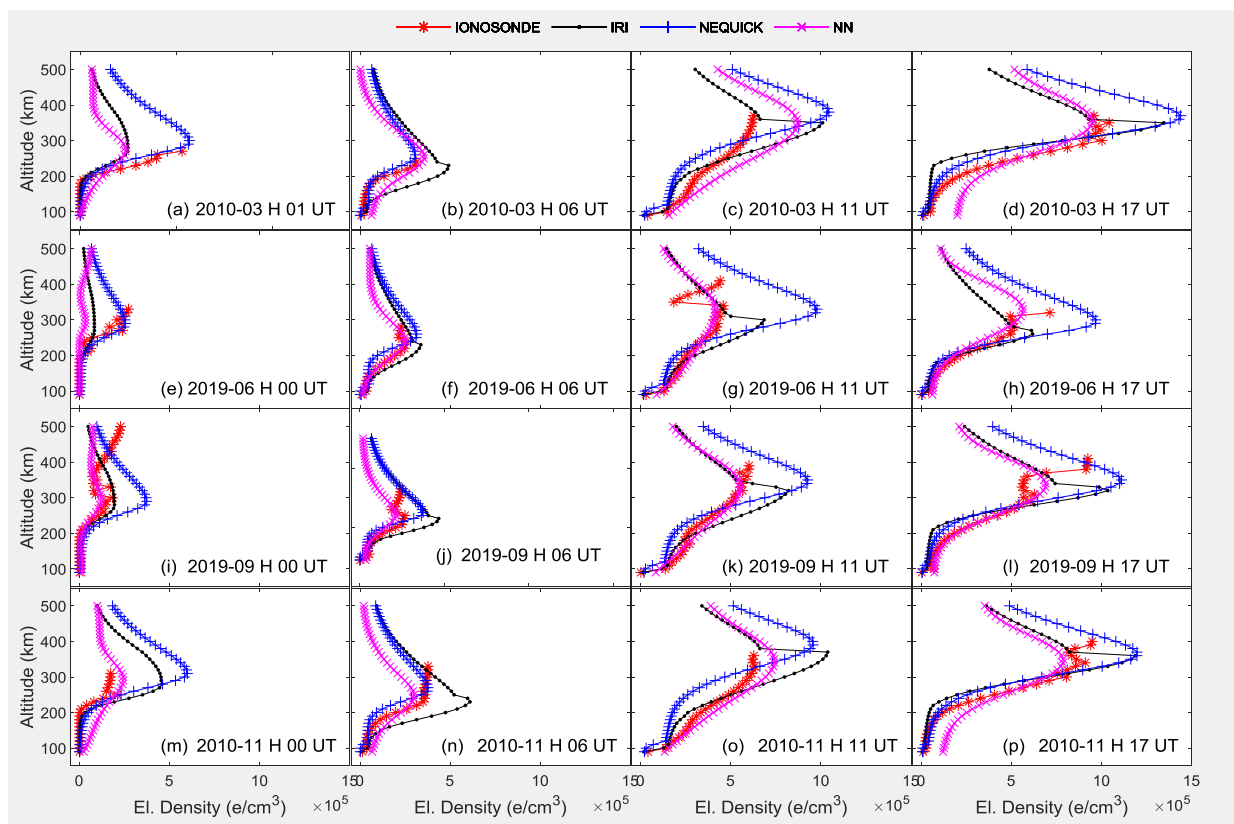


Figure 3. Validation of the NN model predictions with Ionosonde (IL008) Measurements in Comparison to the IRI and the Nequick models' Predictions.

Table 1. Root-Mean Square Errors (RMSE) of predictions of NN, IRI and NeQuick models.

S/N	Month & hour of day	Root Mean Square Error ($\times 10^3$ cm ⁻³)		
		IRI	NeQuick	NN
1	2010-03 H01:00 UT	107	59	106
2	2010-03 H06:00 UT	177	36	77
3	2010-03 H11:00 UT	93	110	132
4	2010-03 H17:00 UT	214	142	127
5	2019 06 H00:00 UT	59	33	87
6	2019 06 H06:00 UT	58	61	11
7	2019 06 H11:00 UT	128	149	25
8	2019 06 H17:00 UT	59	188	47
9	2019 09 H00:00 UT	26	100	22
10	2019-09 H06:00 UT	122	83	40
11	2019-09 H11:00 UT	124	84	39
12	2019-09 H17:00 UT	116	84	26
13	2010-11 H00:00 UT	144	147	79
14	2010-11 H06:00 UT	162	63	69
15	2010-11 H11:00 UT	77	154	61

S/N	Month & hour of day	Root Mean Square Error ($\times 10^3$ cm ⁻³)		
		IRI	NeQuick	NN
16	2010-11 H17:00 UT	117	93	103

The total monthly averages of 423 hourly bin electron density profiles were therefore obtained. The comparison of the hourly binned monthly average electron densities of the IRI, NeQuick, and NN models is presented in Figure 3 and Table 1.

Table 1 and Figure 3 show the results of 16 electron density profiles presented to represent the results of the 423 profiles representing different conditions of times of the day and seasons of the year. It can be observed that the NN model predictions are typically found to be nearest to the ionosonde observations in comparison to those of the IRI and the NeQuick models. The NN model came best in 10 out of the 16 profiles followed by the NeQuick which performed best in 5 out of the 16 profiles then the IRI in 1 out of the 16. The same task was performed on the whole profiles to get more holistic result. The result shows that the NN model was found to be the best of the three models. These can be observed from Figure 4 in which the NN model performed best in 200 cases, the IRI model performed the best in 114 cases, and the NeQuick in 109 cases but the NeQuick had a better standard deviation than the IRI model.

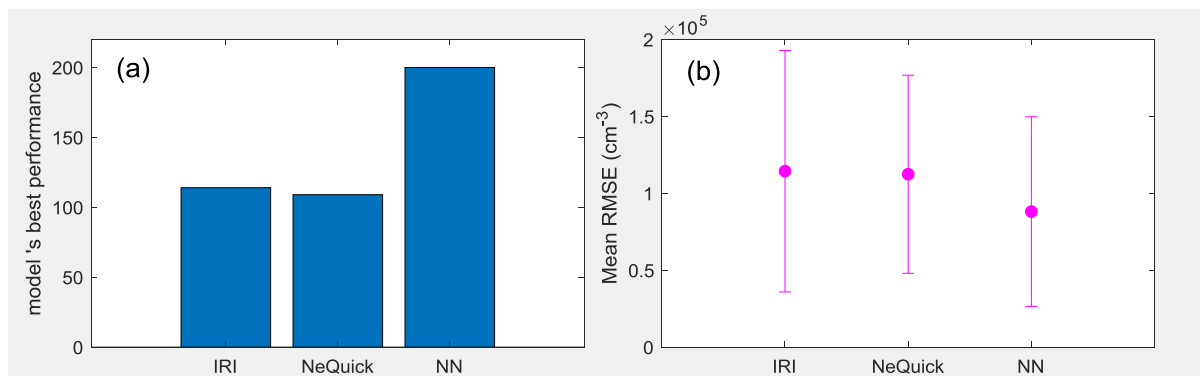


Figure 4. (a) shows the number of profiles in which models performed best. (b) shows the mean of RMSE (the position of the dots in majesty color) and their standard deviations (the length of the error bars).

3.3. Diurnal, Seasonal, and Long-term Ionospheric Variations (the Solar Cycle Changes)

It has been discussed previously in this paper that regular changes in the ionosphere include: diurnal variations, seasonal variations, and long-term variations (the solar cycle

changes). It is earlier explained that the ionosphere changes with the level of solar activities which has a complete cycle in approximately 11 years i.e. its activity goes from trough to peak and to trough again during approximately 11 years.

Figure 5 was constructed to illustrate diurnal, seasonal, as well as long-term ionospheric electron density variations within the entire solar cycle 24 (from the year 2009 to 2019) over Kano, Nigeria. Each row of each of Figure 5 represents diurnal

and seasonal variations of the particular year labeled on it and also illustrates that the ionosphere conspicuously changing with the solar cycle over the location. Figure 5 also reveals that ionization starts to take place around sunrise and increases as the solar zenith angle decreases until saturation is fully established depending on the level of the solar activity of that day. The electron density values remain relatively high due to the presence of sunlight until night. At night, when the solar zenith

angle is high, recombination starts. Since the recombination is a gradual process, the electron density values reduce gradually as the solar zenith angle becomes relatively large (the Sun goes beyond the horizon) consequently, the electron density becomes relatively very low. This reciprocal attitude between the ionosphere and the solar zenith angle is also shown in Figure 5 which also revealed the well-known features of the ionospheric change with solar cycle.

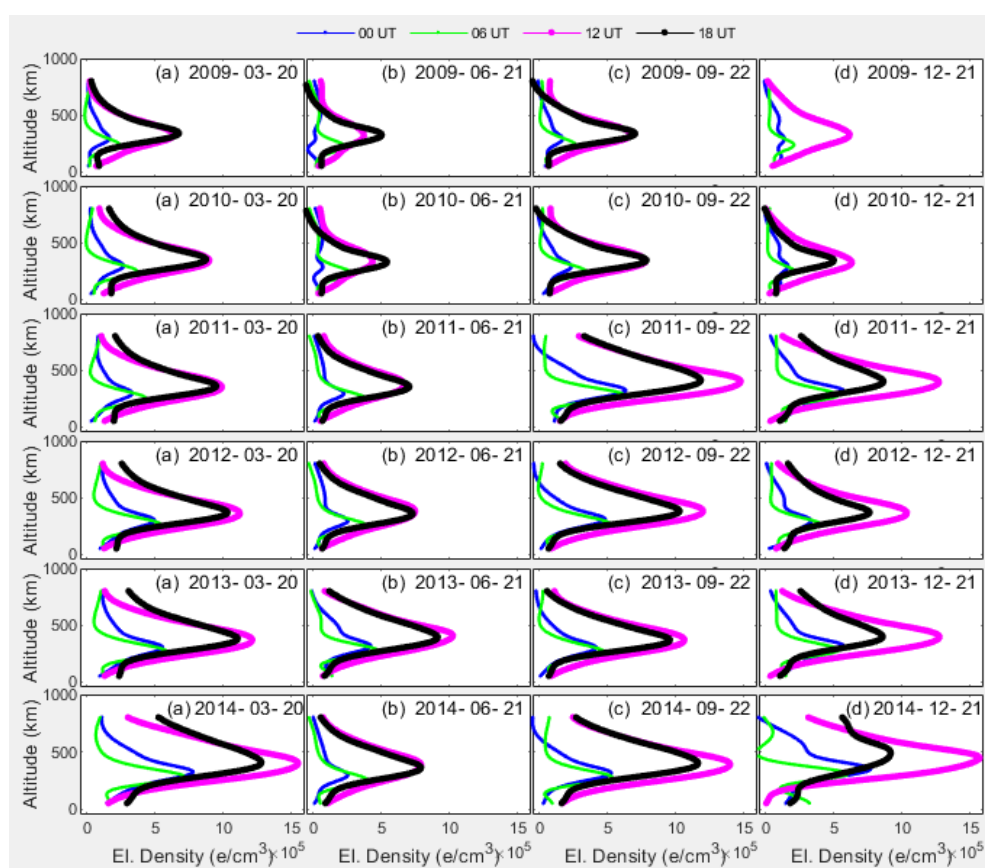


Figure 5. Diurnal and seasonal variations for the solar cycle 24 running from the trough to the peak over Kano, Nigeria. Each row represents the March equinox, June solstice, September equinox, and December solstice days respectively for a particular year.

It is difficult to understand the NmF2 values for the different seasons (March equinox, June solstice, September equinox, and December solstice) presented in Figure 5 by visual inspection. Table 2 and Figures 6-9 was plotted to give these illustrations.

Table 2. Peak electron densities (NmF2) for morning, afternoon, evening, and night of March equinox, June solstice, September equinox, and December solstice days during solar cycle 24.

		2009	2010	2011	2012	2013	2014
Season	Local Time	NmF2 $\times 10^5$	NmF2 $\times 10^5$	NmF2 $\times 10^5$	NmF2 $\times 10^5$	NmF2 $\times 10^5$	NmF2 $\times 10^5$
March Equinox day	00	1.7	2.7	3.3	5.2	5.6	7.8
	06	2.4	3.7	4.4	5.5	5.8	7.1
	12	6.4	9.0	9.9	11.7	12.1	15.5
	18	6.8	8.7	9.5	10.6	11.1	12.8

		2009	2010	2011	2012	2013	2014
Season	Local Time	NmF2 $\times 10^5$	NmF2 $\times 10^5$	NmF2 $\times 10^5$	NmF2 $\times 10^5$	NmF2 $\times 10^5$	NmF2 $\times 10^5$
June solstice day	00	0.6	0.7	2.3	3.0	4.2	2.6
	06	2.3	2.7	3.8	4.0	4.8	3.9
	12	3.7	4.4	6.7	8.2	10.3	7.9
	18	5.0	5.4	7.0	8.0	9.1	7.9
September Equinox day	00	1.7	2.4	6.3	4.6	4.1	5.3
	06	2.7	3.4	6.1	5.0	4.7	5.3
	12	6.7	7.9	14.8	11.1	10.6	14.0
	18	7.0	7.9	11.8	10.0	9.6	11.7
December solstice day	00	1.4	1.7	5.7	2.9	5.7	7.7
	06	2.1	2.2	5.3	3.9	5.3	6.0
	12	6.2	6.3	12.7	10.2	12.6	15.7
	18	4.9	5.0	8.6	7.7	8.6	9.2

The same task was also performed on the remaining year of the solar cycle 24. These Figures demonstrate the NN model's capability to reproduce different ionospheric features (diurnal, seasonal and long-term variations).

Figures 6-9 were constructed to compare the diurnal variations of the NmF2 of different seasons of the entire solar cycle 24 over Kano, Nigeria.

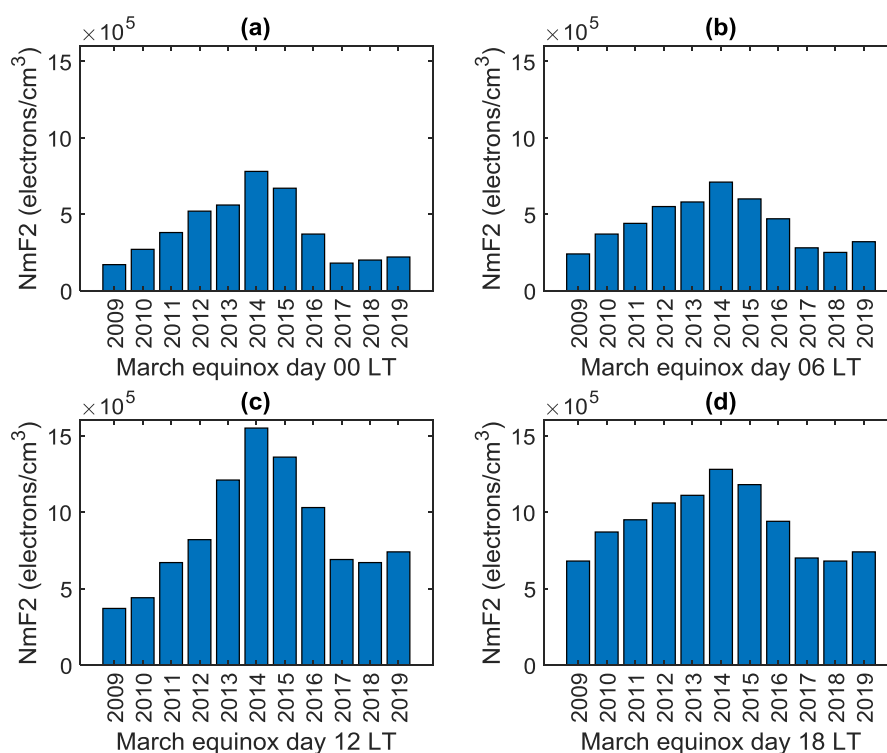


Figure 6. (a) the NmF2 values for universal midnight, (b) universal morning, (c) universal midday, and (d) universal evening of the March equinox days of the entire solar cycle 24 over Kano, Nigeria.

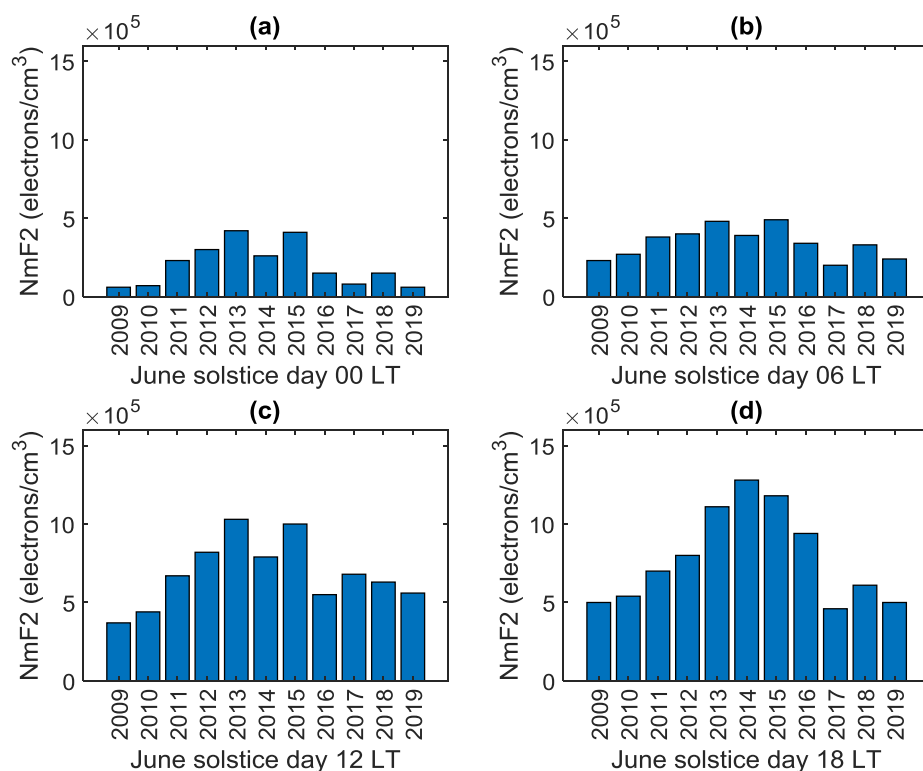


Figure 7. (a) the NmF2 values for universal midnight, (b) universal morning, (c) universal midday, and (d) universal evening of the June solstice days of the entire solar cycle 24 over Kano, Nigeria.

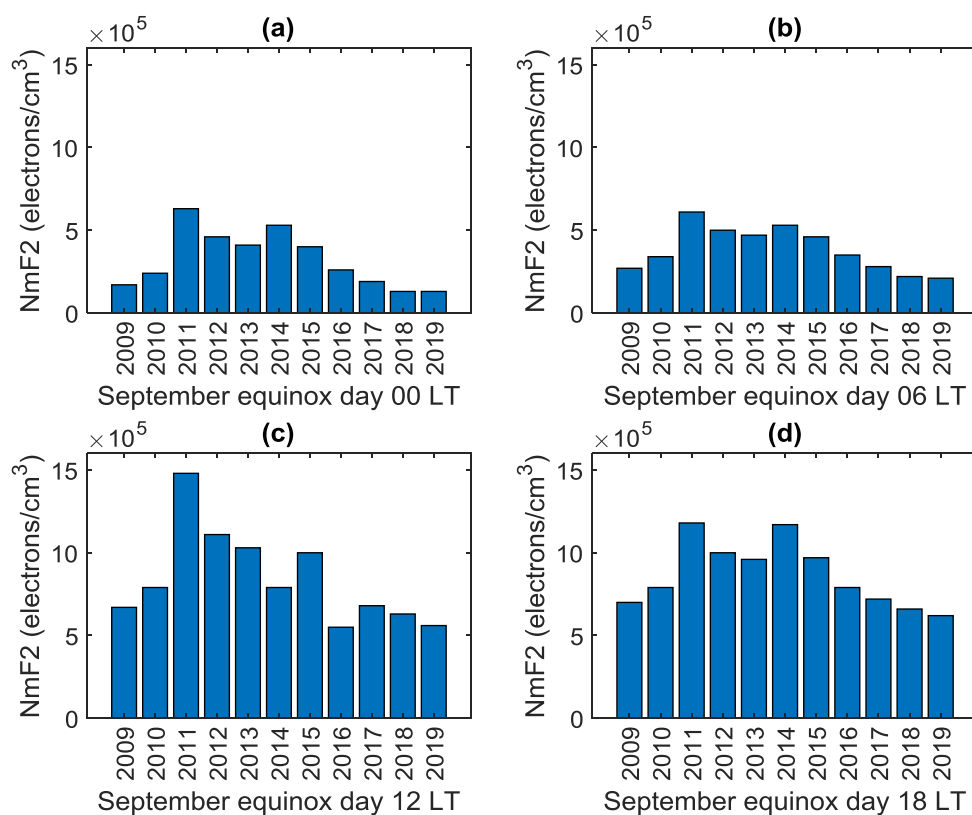


Figure 8. (a) The NmF2 values for universal midnight, (b) universal morning, (c) universal midday, and (d) universal evening of the September equinox days of the entire solar cycle 24 over Kano, Nigeria.

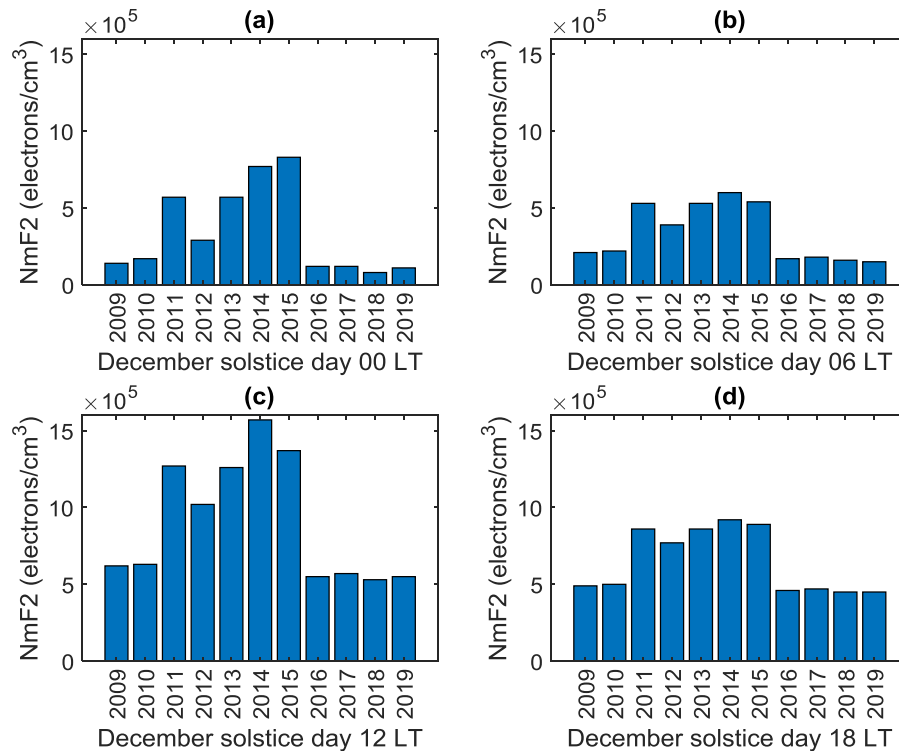


Figure 9. (a) The NmF2 values for universal midnight, (b) universal morning, (c) universal midday, and (d) universal evening of the December solstice days of the entire solar cycle 24 over Kano, Nigeria.

Interestingly, Figures 6–9 display the well-known features of solar cycle 24 with minimal as 2009 and 2019 and with the first peak in late 2011 and maxima in 2014. It also displays the well-known features of the ionospheric. They also reveal that the equinoxes have lower solar zenith angles than the solstices. The NmF2 is generally higher in high solar activity years (HAS) years than in the years of low solar activity (LSA). Looking at the solar cycle 24, which runs from minima to maxima and then to minima again within 11 years, the minima occurred in 2009 and 2019, the Figures show similarities in NmF2 for the years 2009 and 2019. This proves that (i) the Seasonal behavior of NmF2 is dependent on solar activity; (ii) The NmF2 is generally higher in the equinoxes than in the solstices except in the December solstice (especially HSA years) because Nigeria is mostly in the Southern Hemisphere [18] in this season and therefore receive more sunlight.

4. Conclusion

The ionospheric electron density model has been developed using neural network. Data used for the neural network trainings are electron density measurements derived from both COSMIC-1 and COSMIC-2 satellites by radio occultation technique during the periods from 2006 to 2021, in a 5-degree rectangular region around Kano, Nigeria (a station within the equatorial region). In order to establish an optimum result, the best algorithm in terms of prediction accuracy and speed was used. Results for 22 trained networks showed that the network with nineteen hidden layer neurons offer the most

accurate result with root-mean square error (RMSE) of 86×10^3 electrons per cubic centimeter. The nineteenth network was therefore finally used in developing the neural network (NN) model. Validation of the developed NN model was done using ionosonde electron density measurements obtained from Ilorin, Nigeria (another equatorial station, south-west of Kano). Performances of the NN model relative to the ionosonde measurements were also compared alongside those of the NeQuick and IRI models. Analysis of the root-mean square errors of the model predictions relative to the ionosonde measurements showed that the NN model predictions were better than those of the IRI and the NeQuick. In a total of 433 ionosonde electron density profiles used, the NN model predictions presented the least (best) RMSEs in 200 profiles (approximately 47%), the IRI model predictions came second in 114 profiles (approximately 27%), and then the NeQuick model in 109 profiles (approximately 26%). The NeQuick predictions however exhibited lower (better) standard deviation of the RMSEs.

The NN model was also demonstrated to be able to (i) derive continues electron density measurements from the COSMIC measurements which are not continues in time (being one of the limitations of the COSMIC data) and (ii) reproduce the different ionospheric features including diurnal variations, seasonal variations, and long-term variations (variations due to solar activities). The overall better performance of the NN model further supports the idea that neural networks are suitable candidates for contemporary ionospheric modeling in this era of big data.

5. Recommendations

Other methods of ionospheric modelling over this African equatorial region may also be used to investigate whether they are more suitable than the neural network method.

It is recommended that Future research may consider ionospheric data different from COSMIC mission radio occultation measurements to model the ionospheric electron density over this location to compare the two models.

Abbreviations

COSMIC	Constellation Observing System for Meteorology Ionosphere and Climate
LM	Levenberg Marquardt
RMSE	Root-Mean Square Error
NN	Neural Network
IRI	International Reference Ionosphere
TEC	Total Electron Content
GPS	Global Positioning System
RO	Radio Occultation
doy	Day of the Year
Hr	Hour of the Day
UT	Universal Time
IonPrf file format	Ionprf is one of the data products of FORMOSAT-7/COSMIC-2 occultation observation, which includes the ionospheric electron density profiles, the calibrated TEC, geographic longitude/latitude/altitude at perigees, etc.
NetCDF format	NetCDF, or network common data form, is a file format and library for representing and sharing scientific data. it is used to store multidimensional scientific data such as temperature, humidity, pressure, wind speed and direction.
Dst index	The Dst index is an index of magnetic activity derived from a network of near equatorial geomagnetic observatories that measures the intensity of the globally symmetrical equatorial electrojet (the “ring current”).
F10.7	F10.7 or the solar ratio flux at 10.7 cm is a measurement of solar activity that is used in space weather modelling and other applications

Conflicts of Interest

The authors declare no conflicts of interest.

References

- [1] Abubakar, S., Okoh, D., Tijjani, B. I., & Said, R. S. (2024). Speed and accuracy investigations of neural network algorithms for ionospheric modelling at an equatorial region. *Journal of Atmospheric and Solar-Terrestrial Physics*, 265, 106365. <https://doi.org/10.1016/j.jastp.2024.106365>
- [2] Abuelezz, O., Mahrous, A., Cilliers, P., Fleury, R., Youssef, M. et al. (2021). Neural network prediction of the topside electron content over the Euro-African sector derived from Swarm-A measurements. *Advances in Space Research*, 67(4), pp. 1191-1209. <https://doi.org/10.1016/j.asr.2020.11.009>
- [3] Arthur, C. K., Temeng, V. A. and Ziggah, Y. Y. (2020). Performance evaluation of training algorithms in backpropagation neural network approach to blast-induced ground vibration prediction. *Ghana Mining Journal*, Vol. 20, No. 1, pp. 20-33.
- [4] Bhattarai, N., Chapagain, N. P. and Adhikari, B. (2016). Study total electron content TEC and electron density profile observations during geomagnetic storms using COSMIC satellite data. *Discovery*, 2016, 52(250), 1979–1990.
- [5] Bilitza, D. (2001). International reference ionosphere 2000. *Radio Science*, 36(2), 261-275.
- [6] Bilitza, D., & Reinisch B. W., (2008). International reference ionosphere 2007: Improvements and new parameters. *Advances in Space Research*, 42(4). 599–609. <https://doi.org/10.1015/j.ars.2007.07>
- [7] Bilitza, D., and McKinnell, L. A., (2011), International reference ionosphere (iri-2011), paper presented at 2011 iri workshop, *SANSA Space Sci.*, Hermanus, South Africa.
- [8] Bilitza, D., Pezzopane, M., Truhlik, V., Altadill, D., Reinisch, B. W., & Pignalberi, A., (2022). The International Reference Ionosphere Model: A review and description of an ionospheric benchmark. *Reviews of geophysics*, 60(4), e20222RG000792.
- [9] Cömert, Z. and Kocamaz A. F (2017). A syudy of artificial neural network training algorithms for classification of cardiocotography Cömert signals. *Journal of Science and Technology*, E-ISSN 2146–7706.

- [10] Engelbrecht, A. P. (2007). Computational Intelligence. Chichester, UK: John Wiley & Sons, Ltd.
<https://doi.org/10.1002/9780470512517>
- [11] Habarulema, J. B., Okoh, D., Buresovva, D., Rabi, B., Tshisaphungo, M., et al. (2021). A global 3-D electron density reconstruction model based on radio occultation data and neural networks. *Journal of atmospheric and solar-terrestrial physics*. 221 105702. www.elsevier.com/locate/jastp.
- [12] Hundesa, A. (2024). Ionosonde Data Analysis for Precise Study of Ionospheric Electron Density. *Space Sci J*, 1(1), 01-12.
- [13] Lei, J., Syndergaard, S., Burns, A. G., Solomon, S. C., Wang, W., Zeng, Z., et al. (2007). Comparison of COSMIC ionospheric measurements with ground-based observations and model predictions: preliminary results, *J. Geophys. Res.*, 112, A07308, <https://doi.org/10.1029/2006JA012240>
- [14] Liu, L., Zhao, B., Wan, W., Ning, B., Zhang, M. L. and M. H. (2009). Seasonal variations of the ionospheric electron densities retrieved from Constellation Observing System for Meteorology, Ionosphere, and Climate mission radio occultation measurements, *J. Geophys. Res.*, 114, A02302, <https://doi.org/10.1029/2008JA013819>
- [15] Mathworks (2024b). Choose Neural Network Input-Output Processing Functions. Retrieved 24 September 2024 from <https://www.mathworks.com/help/deeplearning/ug/choose-neural-network-input-output-processing-functions.html>
- [16] Mathworks (2024c). mapminmax. Retrieved 24 September 2024 from <https://www.mathworks.com/help/deeplearning/ref/mapminmax.html>
- [17] Mukhtar I. F. and Benjamin W. J. (2020). Performance Evaluation of IRI and Ne-quick-2 models TEC predictions with GPS derived TEC over some Equatorial stations. *Science Journal of Advanced and Cognitive Research*, Vol. 1(1): 23-36, ISSN. 2736-1667.
- [18] Nava, B., Cořson, P., and Radicella, S. M. (2008). A new version of the NeQuick ionosphere electron density model. *Journal of Atmospheric and Solar-Terrestrial Physics*, 70(15), 1856–1862. <https://doi.org/10.1016/j.jastp.2008.01.015>
- [19] Okoh, D. (2018). GPS Modeling of the Ionosphere Using Computer Neural Networks. *Intec Open: Multifunctional Operation and Application of GPS*.
<http://dx.doi.org/10.5772/intechopen.75087>
- [20] Okoh, D., Ambrose, E., Okere, B., McKinnell, L. A. and Okeke, P. N. (2011). A comparison of IRI-TEC with GPS-TEC over Nsukka, Nigeria, paper presented at IRI 2011 Workshop, SANSA Space Sci., Hermanus, South Africa, 10–14 Oct.
- [21] Okoh, D., Habarulema, J. B., Rabi, B., Seemala, G., Wisdom, J. et al., (2020). Storm-time modeling of the African regional ionospheric total electron content using artificial neural networks. *Space weather* 18, e2020SW002525.
<http://dx.doi.org/10.1029/2020SW002525>
- [22] Okoh, D., Owolabi, O., Ekechukwu, C., Folarin, O., Arhiwo, G., Agbo, J., et al. (2016). A regional GNSS - VTEC model over Nigeria using neural networks: A novel approach. *Geodesy & Geodynamics*, 7(1), 19–31.
<https://doi.org/10.1016/j.geog.2016.03.003>
- [23] Okoh, D., Seemla, G., Rabi, B., J. B., Jin, S., et al., (2019). A Neural Network-Based Ionospheric Model over Africa from Constellation Observing System for Meteorology, Ionosphere, and Climate and Ground Global Positioning System Observations. *Journal of geophysical research: space physics*.
<https://doi.org/10.1029/2019JA027065>
- [24] Okoh, D., Yusuf, N., Adedaja, O., Musa, I., & Rabi, B. (2015). Preliminary results of temperature modelling in Nigeria using neural networks. *Weather*, 70(12), 336–343.
<https://doi.org/10.1002/wea.2559>
- [25] Pellicia, F., Bonafoni, S., Basili, P. and Anniballe, R. (2009). Estimation of Tropospheric Profiles Using COSMIC GPS Radio Occultation Data with Neural Network. *European Journal of Remote Sensing*,
<https://doi.org/10.5721/ItJRS20094132>
- [26] Rabi, A. B., Mamukuyomi, A. I., and Joshua, E. O. (2007). Variability of Equatorial Ionosphere Inferred from Geomagnetic Field Measurement. *Bulletin Astronomy Society India*, 1-12.
- [27] Santosa, H. (2018). Modeling and prediction of ionospheric characteristics using nonlinear autoregression and neural network.
- [28] Shehu, M. U., Said, R. S. and Okoro, E. C. (2017). The trend of Ionospheric Total Electron Content near the Equator. *Bayero Journal of pure and applied Sciences*, 10(1): 258–264.
- [29] Wasserman, P. D. (1989). Neural Computing: Theory and Practice. New York, NY, USA: Van Nostrand Reinhold Co.